Arabian Journal of Chemistry (2023) **16**, 104887

King Saud University

Arabian Journal of Chemistry

www.ksu.edu.sa
www.sciencedirect.com

ORIGINAL ARTICLE

Influence of pore structural properties in metal-organic frameworks on the host-guest interaction in drug delivery

Xiao-Wei Yan [a,1], Somayeh Tarasi [b,1], Su-Juan Wang [a,1], Kobra Rostamizadeh [d], Mao-Lin Hu [c,*], Ali Morsali [b,*], Ali Ramazani [e,f,*], Roghayeh Tarasi [g], Yavar Ahmadi [h]

[a] *Guangxi Key Laboratory of Health Care Food Science and Technology, College of Food and Bioengineering, Hezhou University, No. 18 West Ring Road, Hezhou, Guangxi 542899, China*
[b] *Department of Chemistry, Faculty of Sciences, Tarbiat Modares University, P.O. Box: 14115-175, Tehran, Iran*
[c] *College of Chemistry and Materials Engineering, Wenzhou University, Wenzhou 325035, China*
[d] *Zanjan Pharmaceutical Nanotechnology Research Center, Zanjan University of Medical Sciences, Zanjan, Iran*
[e] *Department of Chemistry, Faculty of Science, University of Zanjan, Zanjan 45371-38791, Iran*
[f] *Department of Biotechnology, Research Institute of Modern Biological Techniques (RIMBT), University of Zanjan, Zanjan 45371-38791, Iran*
[g] *Department of Pharmacology, School of Medicine, Shahid Beheshti University of Medical Sciences, Tehran, Iran*
[h] *Department of Basic Sciences, Farhangian University, Tehran 1939614464, Iran*

Received 24 February 2023; accepted 3 April 2023
Available online 18 April 2023

KEYWORDS

Metal-organic frameworks;
Curcumin;
Drug delivery;
HT-29 cancer cells

Abstract Properties of pore structure in Metal-organic frameworks (MOFs) play a key role in the adsorption of target molecules hence are used to improve the efficiency in MOFs. In this study, we synthesized three MOFs with different hydrophilicity, namely TMU-6(RL1), TMU-21(RL2) and TMU-59. Additionally, we studied the effect of hydrophobicity/hydrophilicity of pore in MOFs on the drug delivery and sensing properties. The structure of these frameworks was characterized by XPS, BET, XRD, IR and TG. The DLC and DLE of TMU-6(RL1), TMU-21(RL2) and TMU-59, were determined by (20%, 70%), (18%, 78%) and (3.6%, 13.6%), respectively. Also, the curcumin release reached 74%, 57% and 8% respectively for TMU-6(RL1), TMU-21(RL2)

* Corresponding authors at: Department of Chemistry, Faculty of Sciences, Tarbiat Modares University, P.O. Box: 14115-175, Tehran (A. Ramazani); College of Chemistry and Materials Engineering, Wenzhou University, Wenzhou 325035, China (M. Hu).
E-mail addresses: 00111024@wzu.edu.cn (M.-L. Hu), Morsali_a@modares.ac.ir (A. Morsali), aliramazani@znu.ac.ir (A. Ramazani).
[1] These authors contributed equally to the manuscript.
Peer review under responsibility of King Saud University.

Production and hosting by Elsevier

https://doi.org/10.1016/j.arabjc.2023.104887

and TMU-59 after 100 h in PBS solution with pH 7.2 respectively. The carriers showed high adsorption efficiency and controlled release. Adsorption of curcumin as an anticancer drug to the MOFs was done through multiple mechanisms such as $_{Host}\pi$–π_{Guest} interaction and $_{Host}$N–H···O$_{Guest}$ hydrogen bonds. Also, studies of in vitro anticancer revealed that the cytotoxicity of the MOFs@Curcumin composites against HT-29 cancer cells in MOFs was more than free curcumin. The findings demonstrated that the changes in the hydrophilic properties of frameworks can specifically control the Host-Guest interactions, drug loading and its release.

1. Introduction

In recent years, cancer has become one of the most challenging issues worldwide, owing to its fast growth and shortage of targeted therapies (Larsen et al., 1988; Siegel et al., 2017; DeSantis et al., 2019). To improve drug accumulation in tumors, several drug delivery methods such as hydrogels, liquid crystals, nanospheres, liposomes, and micelles have recently been developed (Kubra et al., 2021; Awual, 2017; Kubra et al., 2021; Awual, 2019; Ghorbanloo and Tarasi, 2017; Xu et al., 2023; Arora et al., 2023; Awual, 2019; Salman et al., 2021; Awual, 2019; Kubra et al., 2021; Awual et al., 2015). Nevertheless, such drug delivery techniques continue to have disadvantages, including low stability and toxicity issues (Xue et al., 2019). As a result, developing an effective drug delivery technique is critical (Cai et al., 2020; Hasan et al., 2021). MOFs are a class of crystalline nanoporous structures consisting of organic ligands and metal ions (Yaghi et al., 2003; Gao et al., 2020; Xue et al., 2018). MOFs have shown high potential for a wide variety of uses such as sensing, gas storage, separation, drug delivery and catalysis (Tarasi et al., 2022). MOFs are suitable nanocarriers in drug delivery systems due to their variable pore size, excellent biocompatibility, exceptional porosity, and large surface area. One of the important features that have recently been considered in improving the usefulness of MOFs is the hydrophobicity and hydrophilicity of the pore surfaces of MOFs. The presence of hydrophobic or hydrophilic functional groups in these frameworks is one of the main ways for creating hydrophobic or hydrophilic MOFs. With small changes on the structures and incorporation of these functional groups in the linkers (for example, trifluoromethyl groups and alkyl chains, methyl group) in the linkers, one can witness large changes in the hydrophilic and hydrophobic activity of MOFs (Rodríguez-Hermida et al., 2016; Roy et al., 2016; Kim and Huh, 2016). Research has demonstrated that the addition of methyl group to ligands in MOFs greatly improves CO_2 absorption (Liu et al., 2011). Farrusseng and colleagues also showed that they could alter the hydrophilic-hydrophobic balance by post-synthetic alteration, resulting in competitive adsorption of reactants and products and therefore enhancing the catalytic efficiency of the Knoevenogel process (Aguado et al., 2011). The effect of the hydrophilic and hydrophobic properties of MOFs on the drug delivery process is one of the most key and fundamental parameters that has attracted the attention of researchers in recent years. As an instance, the investigation by Horcajada and colleagues in this field showed that drug absorption in MOF could be controlled by the hydrophobic/hydrophilic balance between drugs and MOFs (Rojas et al., 2018). To address this issue, we synthesized three zinc pillared layer MOFs decorated with amine functional groups, namely TMU-6(RL1) ([Zn(oba)$(RL1)_{0.5}]_n$.$(DMF)_{1.5}$), TMU-21(RL2) ([Zn(oba)$(RL2)_{0.5}]_n$.$(DMF)_{1.5}$), and TMU-59 ([Zn(oba)$(RL3)_{0.5}]_n$.$(DMF)_{1.5}$). Curcumin drug was selected as anticancer drug for this study. Curcumin manifests a range of activities such as anti-carcinogenic, anti-oxidant, anti-HIV and anti-inflammatory (Zhou et al., 2011; Awual, 2015) (Fig. 1). However, free curcumin cannot be used because of high hydrophobicity and poor bioavailability; therefore, efficient carriers are required for the usage of the therapeutic value of curcumin (Zheng et al., 2015). On the other hand, excessive curcumin dose can have negative impacts on the body such as increasing prooxidant activity on DNA and decreasing levels of intracellular ATP (Ziyatdinova et al., 2012; Chan et al., 2006). Given all these issues, it seems necessary to detect curcumin with fast and reliable testing.

2. Experimental section

2.1. Materials

All starting materials, including Zinc (II) nitrate hexahydrate 1, 1′-Carbonyldiimidazole, 4, 4′-oxybis (benzoic acid) (H2OBA) were purchased from Aldrich and Merck Company and used as received. The ligands RL1, RL2 and RL3 were synthesized according to previously reported methods.

2.2. Preparation of TMU-6(RL1), TMU-21(RL2) and TMU-59

TMU-6(RL1), TMU-21(RL2) and TMU-59 were previously synthesized (Tarasi et al., 2018; Tarasi et al., 2021). The RL1, RL2 and RL3 ligands, H_2OBA and Zn $(NO_3)_2{\cdot}6H_2O$ were used to synthesize TMU-6(RL1), TMU-21(RL2) and TMU-59 under solvothermal conditions. TMU-6(RL1): FT-IR (KBr pellet) selected bands 653 (m), 775(m), 876(m), 1015 (m), 1086(m), 1158(s), 1231(vs), 1403(vs), 1511(m), 1607(vs), 1680(m), 2855(s), 2923 (w) and 3371(w) cm^{-1}. TMU-21 (RL2): FT-IR (KBr pellet) selected bands 655(m), 774(m), 875(m), 1013(m), 1087(m), 1157(m), 1238(vs), 1405(vs), 1508 (w), 1608(vs), 1681(s), 2852(w), 2922 (w) and 3433(w) cm^{-1}. TMU-59: FT-IR (KBr pellet(644(v), 776(s), 874(v), 1013(m), 1095(v), 1162(v), 1234(s), 1403(vs), 1506(vs), 1612(vs), 1672 (m), 3063(v) and 34076(s) cm^{-1}. The pillar linkers of RL1, RL2 and RL3 were synthesized according to the procedures mentioned in the published process (Fig. 2) (Abedi et al., 2016; Tarasi and Morsali, 2021).

2.3. Characterization

The following devices were utilized to characterize the products. Melting points were measured on an Electrothermal

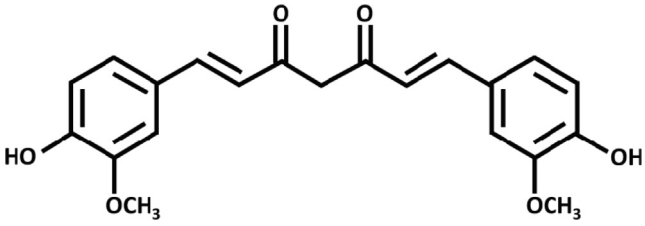

Fig. 1 Chemical structure of curcumin.

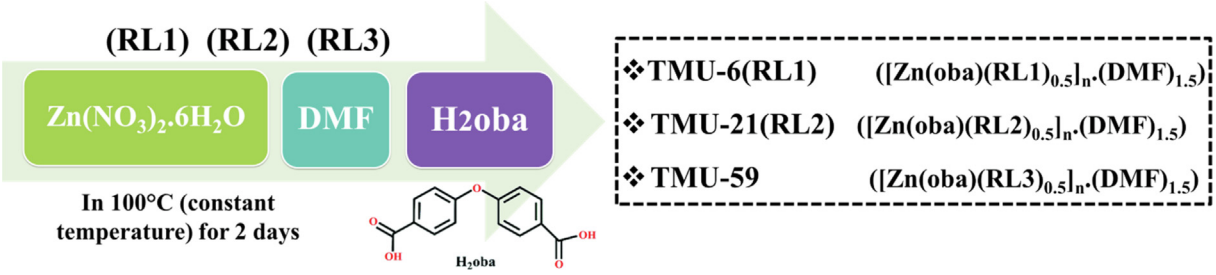

Fig. 2 Method of synthesis of TMU-6(RL1), TMU-21(RL2) and TMU-59.

9100 apparatus. FT-IR spectra were recorded using Thermo Nicolet IR 100 FT-IR. The thermal behavior was measured with a PL-STA 1500 apparatus with the rate of 10 °C.min^{-1} in a static atmosphere of argon. X-ray powder diffraction (XRD) measurements were performed using a Philips X'pert diffractometer with mono chromated Cu-Kα radiation. The 1H NMR spectrum was recorded on a Bruker AC-250 MHz spectrometer at ambient temperature in d6- DMSO and D2SO4. The samples were also characterized by field emission scanning electron microscope (FE-SEM) SIGMA ZEISS and TESCAN MIRA with gold coating (Hasan et al., 2023; Mazrouaa et al., 2019; Awual and Yaita, 2013; Awual, 2019).

2.4. Drug loading measurement

At first, 4 mg curcumin was added to 5 mL ethanol to dissolve completely. Then, an activated sample of MOFs (4 mg) was added. After mixing, the solution was further stirred at room temperature for 24 h, and particles were separated by centrifugation (10000 rpm, 10 min). In addition, for removing free curcumin, particles were washed with excess ethanol. The samples of MOFs@Curcumin composites were dried under vacuum for 12 h at room temperature. The curcumin calibration curve was drawn using a series of standard solution of curcumin by calculating the absorbance at 420 nm. Then, to investigate the amount of curcumin loaded on MOFs, the adsorption reaction was monitored by UV/vis spectroscopy.

2.5. Drug release measurement

The release profile of curcumin was studied in PBS at pH 7.4. The synthesized MOFs@Curcumin composites (5 mg) were dispersed in a PBS (20 mL); then, the solution was put in a shaker at 37 °C (Stirring rates: 100 rpm). Each time, 2 mL of PBS was taken out from the parent solution at fixed time intervals and replenished with fresh PBS. The concentration of curcumin was determined by UV – vis spectrophotometer at 420 nm.

2.6. Fluorescence measurements

The Fluorescence properties of TMU-6(RL1), TMU-21(RL2) and TMU-59 were measured in water containing MOFs using a PerkinElmer-LS55 Fluorescence Spectrometer at room temperature. In a typical procedure, 1 mg of an activated MOF was grinded down, and then immersed in different curcumin solutions (4 mL), followed by testing it in the emission mode after 1 h.

3. Results and discussion

3.1. Characterization of the MOFs

In this work, TMU-6(RL1), TMU-21(RL2) and TMU-59 structures were selected to evaluate the effect of MOF hydrophobicity/hydrophilicity on drug loading, drug delivery, and sensory properties. According to previous reports, MOFs were solvo-thermally synthesized by the reaction of $Zn(NO_3)_2$·$6H_2O$, H_2OBA, RL1, RL2 and RL3 orderly in DMF solvent at 100 °C for 73 h (Fig. 3) (Tarasi et al., 2018; Tarasi et al., 2020; Tarasi et al., 2021).

The TMU-59 structure has small pores of around 5.2 × 6.9 Å, while TMU-6(RL1) and TMU-21(RL2) structures have larger pores of about 7.5 × 6.4 Å (Fig. 4). According to previous reports, the PXRD and SEM were used to examine the structures stability, and the results indicated that the structures were still robust after 24 h in water (Fig. 5a) (Tarasi et al., 2018; Tarasi et al., 2020; Tarasi et al., 2021). To investigate surface area and porosity of MOFs, N_2 adsorption/desorption

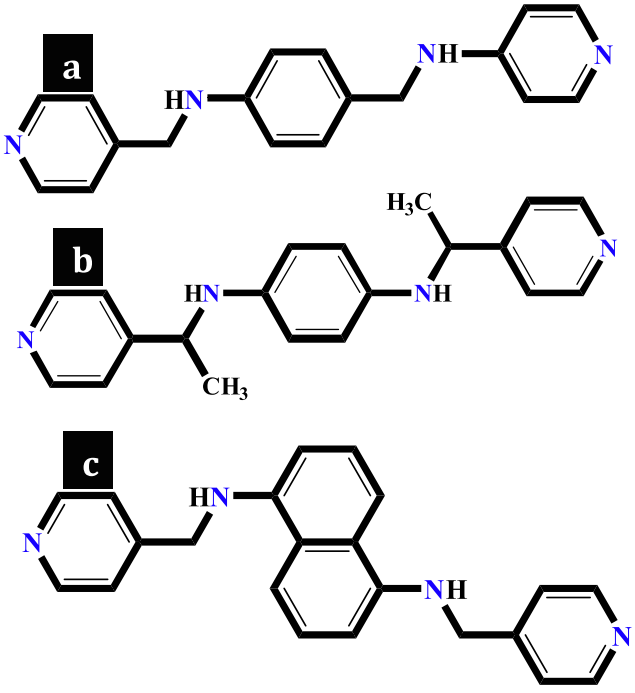

Fig. 3 Views of the (a) RL1 ligand in TMU-6(RL1), (b) RL3 ligand in TMU-59 and (c) RL2 ligand in TMU-21(RL2).

was performed at 77 K and 1 bar on samples. The results displayed that all three MOFs were nonporous to N_2 but were porous to CO_2 at 273 k [Brunauer-Emmett-Teller (BET) surface area of 129 and 94 m^2/g, for TMU-21(RL2) and TMU-21(RL2), respectively] (Fig. 5b, c and d). The pore size distribution revealed a narrow distribution of about 7.5 Å × 6.1 Å for both TMU-6(RL1) and TMU-21(RL2) (Fig. 5e). This is consistent with the pore size determined by X-ray crystallographic study structures, which is around 7.5 Å × 6.4. This suggests that TMU-6(RL1) and TMU-21(RL2) are flexible or breathing frameworks, explaining why both are nonporous to N_2, yet, adsorb CO_2 and pharmacological guest molecules. At 77 K, N_2 sorption is measured. At this cryogenic temperature, N_2 cannot permeate minuscule holes. CO_2 and drug adsorption occur at room temperature, where the framework's thermal and vibrational flexibility allows for the inclusion of even large guest molecules.

3.2. Thermal analysis of TMU-6(RL1), TMU-21(RL2) and TMU-59

The results of thermogravimetric analysis show that the structures TMU-6(RL1) and TMU-21(RL2) lose their weight at three different temperatures. The first weight loss occurs at 100 °C and is associated with the desorption of physically adsorbed water molecules inside the framework pores. The second weight loss occurs at 100–380 °C, which is associated to the removal of DMF guest molecules, and the final weight loss occurs in the temperature range of 380–400 °C and corresponds to the degradation of frameworks. Additionally, the

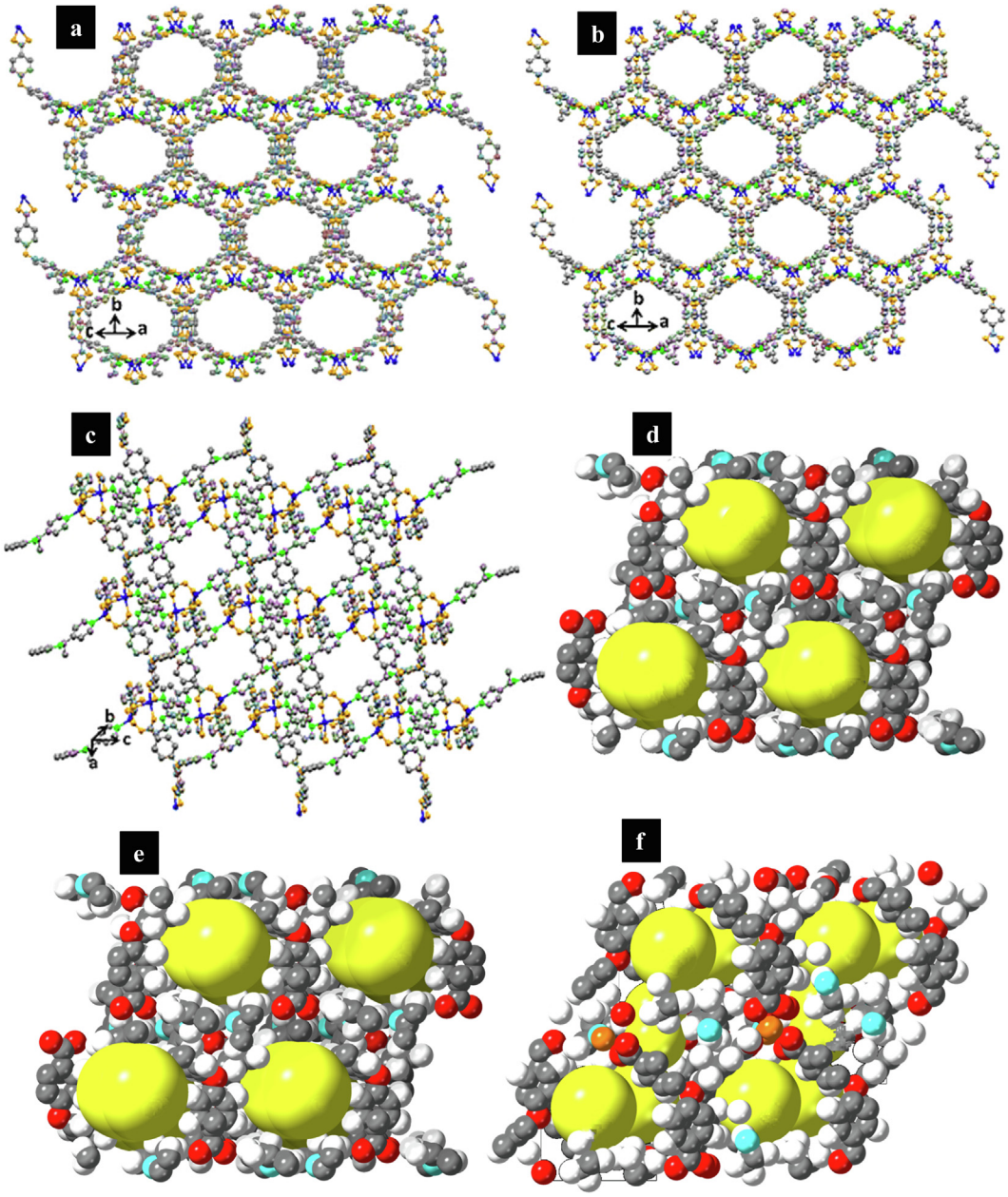

Fig. 4 Representation of the pores, (a) TMU-6(RL1), (b) TMU-21(RL2) (c) TMU-59 (Zinc: Blue, Carbon: Gray, Oxygen: Orange, Green: Nitrogen). Representation showing the pore channels (yellow balls) (d) TMU-6(RL1), (e) TMU-21(RL2) (f) TMU-59.

thermogravimetric analysis showed that TMU-21(RL2) is slightly more thermally stable than TMU-6(RL1) (Fig. S2). Also, the thermogravimetric analysis on the synthesized of TMU-59 exhibit that the weight loss (17.8%) is attributed to the extraction of DMF solvent molecules in the temperature range of 50–250 °C (calculated 18%, find about 17.8%). The principal loss steps occur between 390 and 440 °C during the decomposition of the framework. After that, about 25 percent weight remains (which is belong to the metal section of the structure) and the organic fraction entirely decomposed. Accordingly, the remaining portion could probably be the ZnO. The general weight loss in the temperature range of

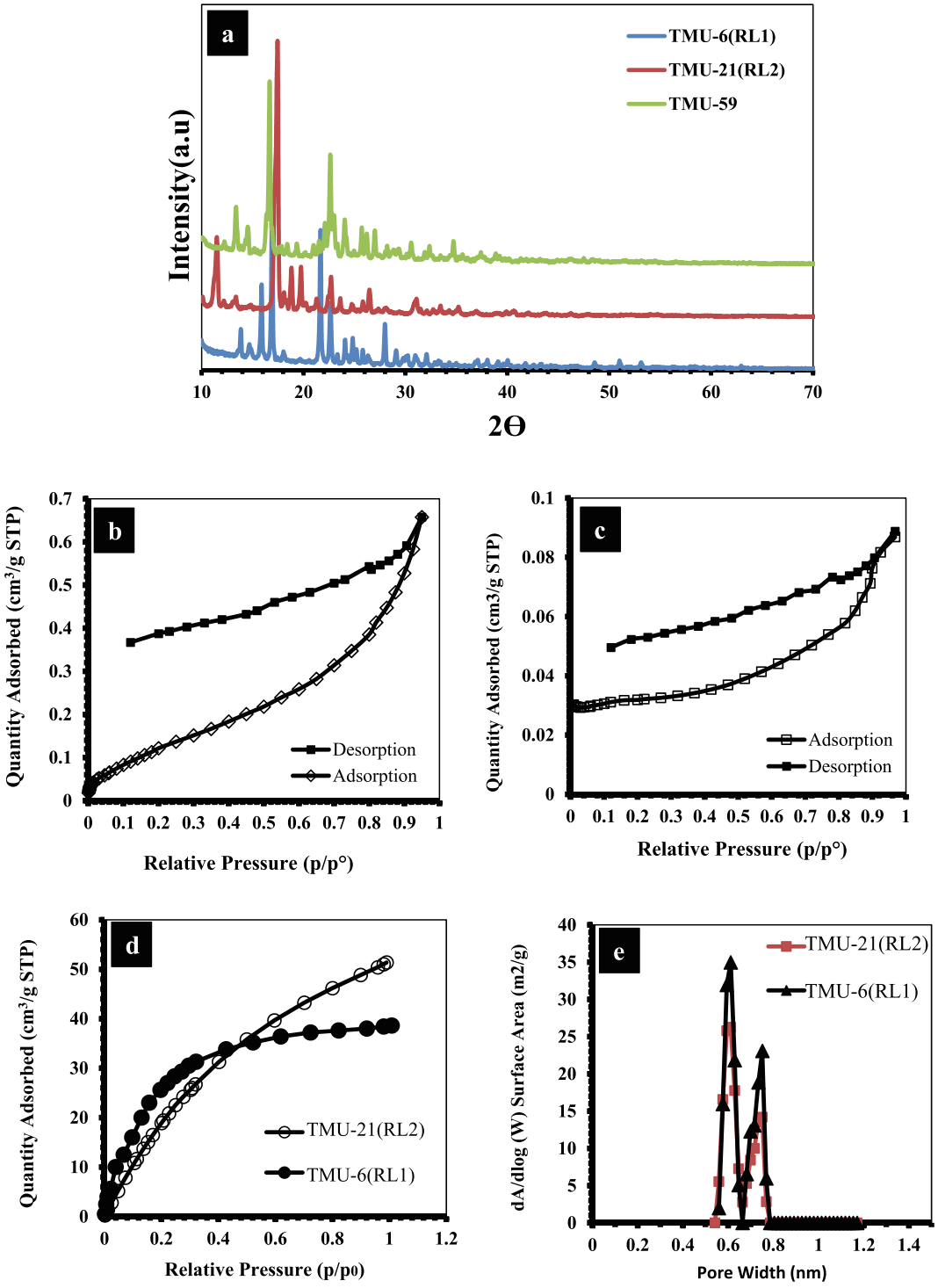

Fig. 5 N_2 adsorption–desorption isotherms of (b) TMU-6(RL1) and (c) TMU-21(RL2), (d) CO_2 isotherms collected at 273 K of TMU-21(RL2) and TMU-6(RL1), (e) Pore size distributions of TMU-6(RL1) and TMU-21(RL2).

50–450 °C about 75 % is near to the calculated amount of 76 %. Accordingly, during the basic weight loss steps TMU-59 is fully decomposed to an uncertain metallic structure which is in accordance with the TGA results (Fig. S3).

3.3. Drug release study

The amount of loaded drug for the three structures was obtained based on the results of the adsorption experiment as well as the following equations (Fernández-Bravo and Figueras, 2020) (Table S1) (Fig. S8).

Drug loading encapsulation efficiency (DLE)%

= (Total amount of loaded drug/Initial amount of drug) × 100%.

Drug loading capability(DLC)%

= (Total amount of loaded drug/Total amount of MOFs) × 100%

According to the procedure described for drug loading and drug release in supporting, the DLC and DLE for TMU-6 (RL1), TMU-21(RL2) and TMU-59 were determined by (20%, 70%), (18%, 78%) and (3.6%, 13.6%), respectively. The curcumin release reached 57%, 74% and 8% for TMU-6(RL1), TMU-21(RL2) and TMU-59 after 100 h in PBS solution with pH 7.2, respectively (Fig. 6a). The pillar linkers in TMU-6(RL1) and TMU-59 had a phenyl core, whereas 2 have a naphthalene core (Fig. 3). Furthermore, because of the presence of phenyl or naphthyl cores around the interaction site, these MOFs have different hydrophilicity properties. The contact angle of the structures was specified using a contact angle analysis to determine the extent of hydrophilicity (Fig. S11). According to the results, the hydrophilicity of MOFs is in the sequence TMU-6(RL1) > TMU-21(RL2) > TMU-59. Also, the hydrophilicity of MOFs@Curcumin Composites is as follows: TMU-6(RL1)@Curcumin > TMU-21(RL2)@Curcumin > TMU-59@Curcumin. Although TMU-59 is the most hydrophobic, had the lowest loading and release of curcumin. This phenomenon might be attributed to having a smaller pore due to the presence of methyl groups, resulting in a weak interaction between TMU-59 and curcumin. Based

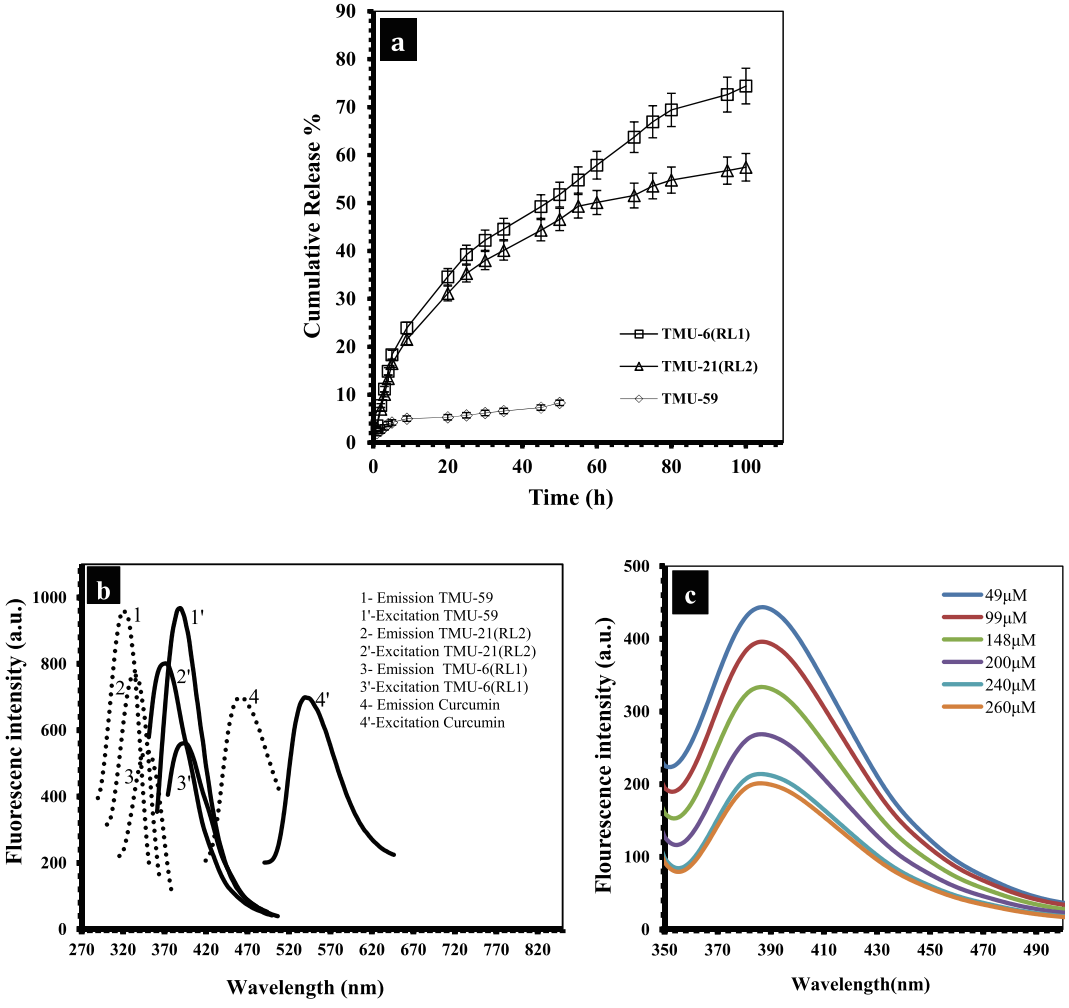

Fig. 6 (a) Curcumin release profiles from MOFs@Curcumin in PBS solution (pH 7.4), (b) The maximum emission and excitation spectra of TMU-6(RL1), TMU-21(RL2), TMU-59 and curcumin in water. (c) Fluorescence emission spectra of TMU-21(RL2) dispersed in water at different concentrations of curcumin.

on these findings, the TMU-21(RL2) structure, with lower hydrophilicity, more developed π-system and high percentage of interaction with guests, showed better interaction with hydrophobic drug curcumin than TMU-6(RL1) and performed better in drug absorption and sensing. However, TMU-21(RL2) had a much stronger interaction with the drug compared with TMU-6(RL1); hence the rate of drug release by TMU-21(RL2) structures was lower. As a result, TMU-6

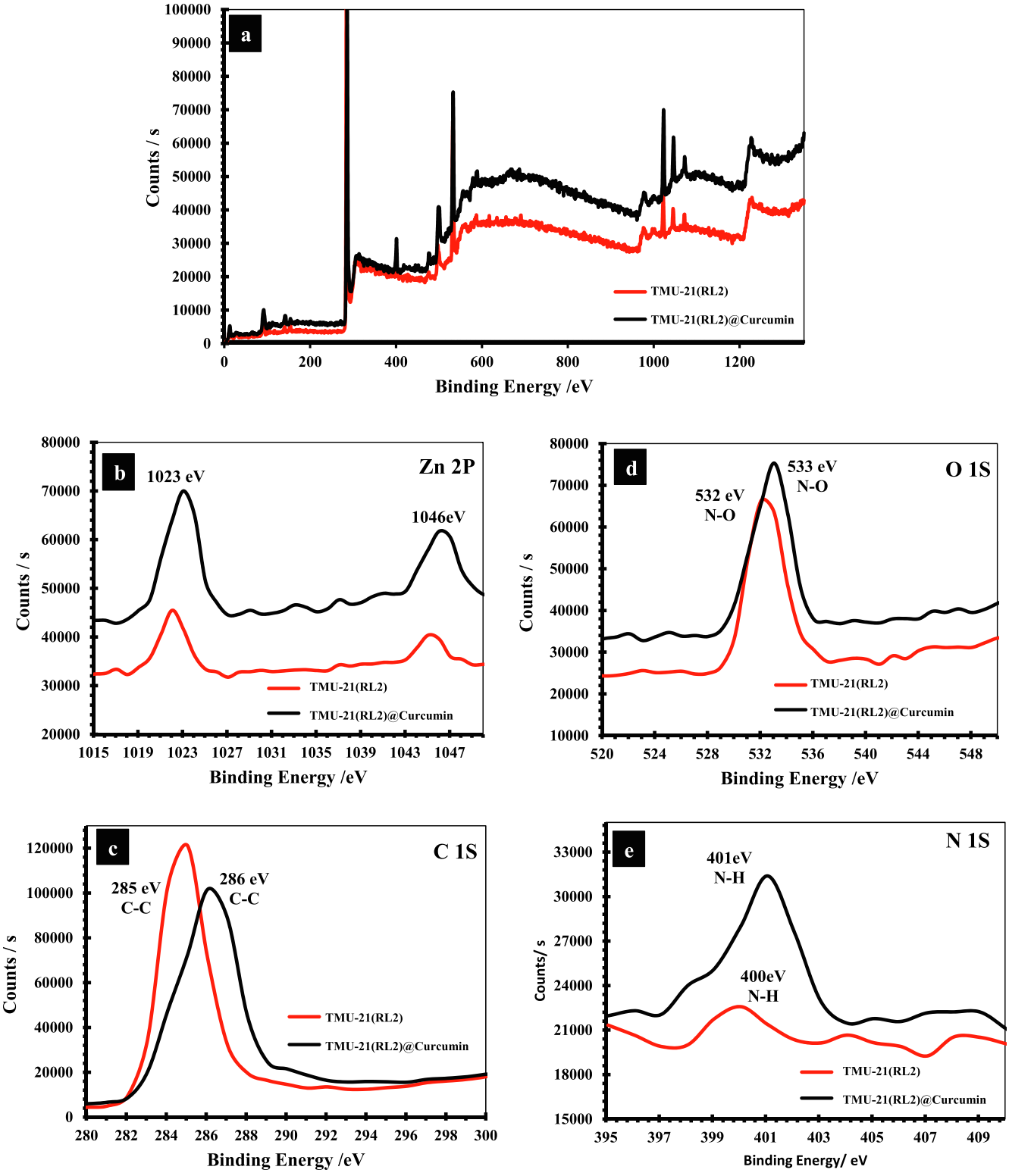

Fig. 7 (a) XPS survey spectrum and high resolution XPS spectra of (b) Zn 2p (c) C 1s, (d) O 1S, and (e) N 1S of TMU-21(RL1) respectively.

(RL1), which has higher hydrophilicity and drug release, was found to be a better carrier for curcumin than the other two MOFs.

3.4. Curcumin sensing

Also, the photoluminescence ability of three activated MOF in water was studied. TMU-6(RL1), TMU-21(RL2) and TMU-59 displayed maximum absorbance in the solid-state UV–Vis spectra at 335 nm, 337 nm, and 300 nm, respectively (Fig. S1). MOFs excitation/emission wavelengths were as shown in Fig. 6b. The quenching efficiencies (Ksv) were obtained according to the Stern-Volmer (SV) equation: $(I_0/I) = K_{SV}[A] + 1$. The quenching efficiency of three structures in the presence of curcumin is as follows: TMU-21(RL2) > TMU-6(RL1) > TMU-59 (Figs. 6c, S5, S6 and S7). TMU-21 (RL2) has a higher K_{SV} value than TMU-6(RL1) and TMU-59 ($K_{SV} = 1 \times 10^6$, 42958, and 8740 M^{-1} for TMU-6(RL1), TMU-21(RL2) and TMU-59, respectively).

3.5. Investigating curcumin sorption in MOFs

An XPS examination was also carried out to offer more information on the sorption mechanism. Some peaks in the high resolution XPS spectra of MOFs moved to higher binding energies following adsorption of curcumin, indicating that curcumin has been bound with the framework (Fig. 7, S9 and S10). SEM was applied to study the stability of the frameworks after curcumin loading, and the results revealed that the that the structures remained stable after drug adsorption and no changes in the structures after drug absorption are observed in the SEM images (Fig. S4).

3.6. Theoretical calculations

To better investigate the interface between substrate interactions with different ligands in MOFs, we first analyzed the Molecular electrostatic potential (MEP) plots of the isolated ligands. MEP maps are a clear criterion for understanding the most reactive electrophilic and nucleophilic sites of molecules. In the MEP diagram, the most electropositive potential (atoms in this region have a tendency to donate electrons (nucleophilic)) and the most electronegative potential (atoms in this region have a tendency to attract electrons (electrophilic)) are shown with blue and red (or yellow) colors, respectively. Areas where the potential is zero are shown in green. Therefore, to investigate the relationships of curcumin with different ligands in the MOFs with the aim of better understanding the interactions between them, we first used theoretical calculations to study the MEP diagrams of individual ligands and curcumin. Fig. 8 depicts the MEP isosurfaces of these compounds on the 0.001 au electron density isosurface, where negative and positive areas represent electrophilic and nucleophilic sites, respectively. Ligands RL1, RL2, and RL3 each have a positive and negative area connected to amine and pyridine nitrogen atoms, respectively. Fig. 8 shows that the positive MEP areas in RL1, RL2, and RL3 are connected with amine nitrogen atoms, indicating that these sites have the ability to attack an electrophilic site (C═O group) in curcumin drug. The interaction between the curcumin drug and the ligands was entirely validated by this computational technique.

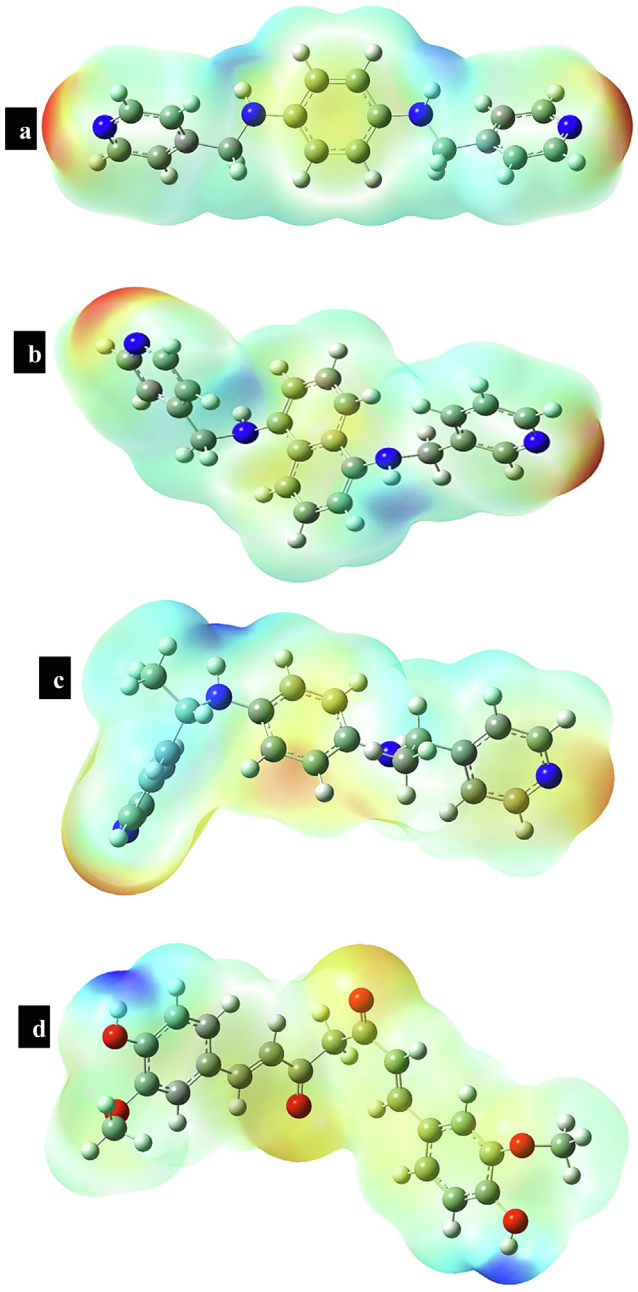

Fig. 8 Electrostatic potentials mapped on the electron isodensity surface of ligand (a) RL1, (b) RL2, (c) RL3 and (d) Curcumin.

3.7. Cytotoxicity study in cancer cells

In vitro anticancer studies were conducted to examine the therapeutic effectiveness of curcumin loaded in MOFs. To determine the remedial effect of curcumin placed in MOFs, in vitro anticancer tests were carried out. To distinguish between a compounds biocompatibility and in vitro cytotoxicity, a cytotoxicity test (MTT test) was first utilized. The survivals of TMU-6(RL1), TMU-21(RL2), TMU-59, RL1, RL2, and RL3 cells were investigated using the human fibroblast-derived cell line. The results revealed that the TMU-6(RL1), TMU-21(RL2), TMU-59, RL1, RL2, and

RL3 in various doses and for 24 h do not appear to be cytotoxic (Fig. 9a). The tests revealed that the MOFs had no significant cytotoxicity. Additionally, utilizing a cytotoxicity test on the cancer cell line HT-29, we assessed the cytotoxic effects of the composites TMU-6(RL1)@curcumin, TMU-21(RL2)@curcumin, and TMU-59@curcumin were assessed. Fig. 9b demonstrates how free curcumin and MOFs@curcumin composites, at concentrations of 100, 200, and 500 g/L over 24 h, internment of reproduction of HT-29 cells. The outcomes also showed that MOFs@curcumin composites inhibited HT-29 and cell proliferation more so than free curcumin. This demonstrates that MOFs can enhance curcumin bioavailability by increasing curcumin transport to cancer cells. TMU-6(RL1) structure has a higher curcumin release compared to TMU-21(RL2) and TMU-59, which improves the ability of the structures to inhibit cancer cells. In following, intracellular uptake ability of curcumin loaded TMU-6(RL1) was evaluated. For this purpose, curcumin loaded MOF which possessed some

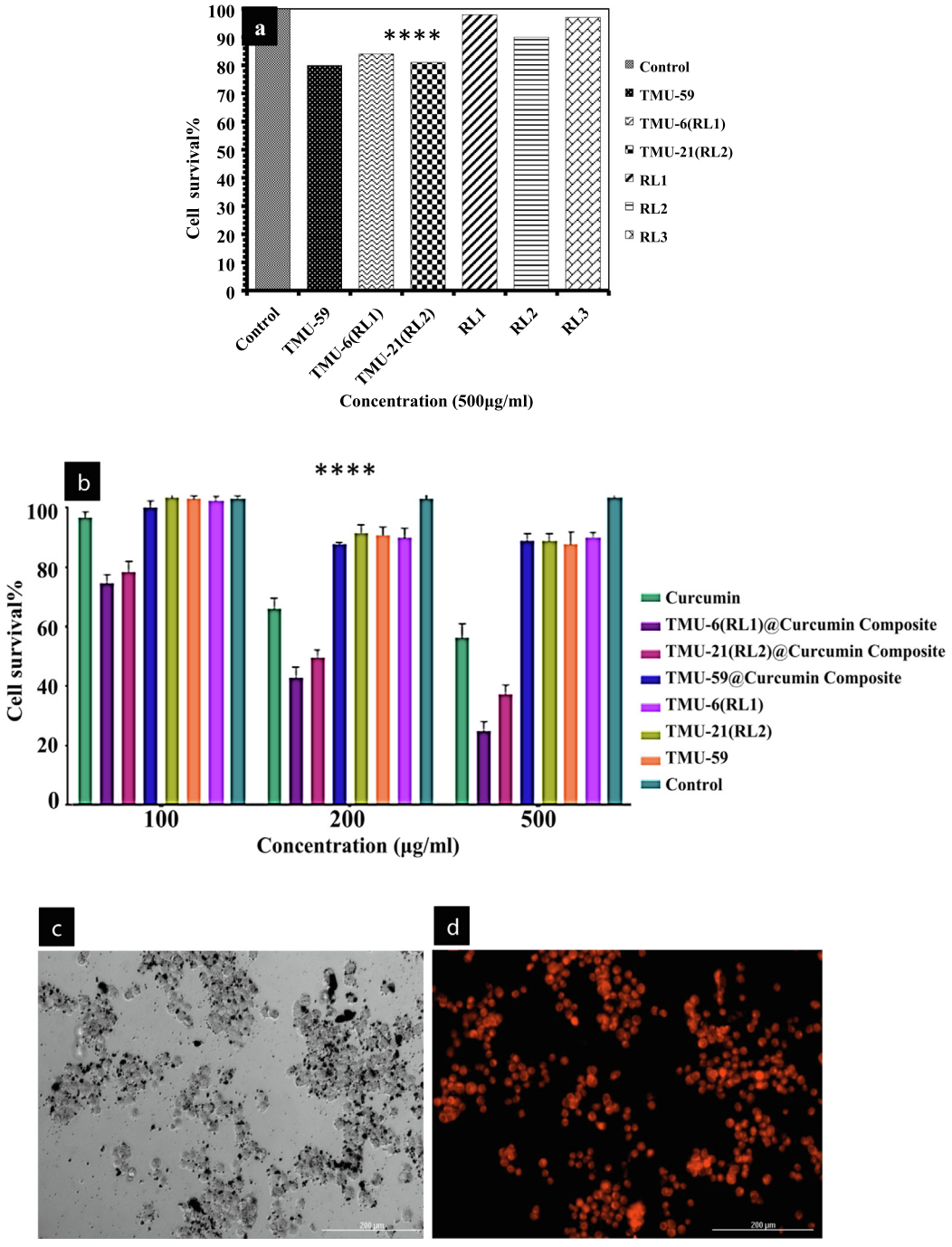

Fig. 9 (a) Cytotoxicity of the ligands and MOFs, (b) Viability of HT-29 cells incubated with MOFs@Curcumin composites and free drug for 24 h. Fluorescence microscopy images of HT-29 cells incubated with: TMU-6(RL1)@Curcumin for 4 h at 37 °C, (c) bright field, (d)fluorescence field.

free sites, was incubated with rhodamine B to tag the nanocarrier. Then, the HT-29 cell line was treated with rhodamine B tagged curcumin loaded TMU-6(RL1) for investigation of intracellular uptake ability of the MOF. After 4 h incubation at 37 °C, the cells were evaluated using fluorescent microscopy. The cytoplasm of all HT-29 cells was highly fluorescent due to the presence of rhodamine B tagged MOF. In addition, rhodamine B tagged MOF demonstrated cellular uptake about 90% after 4 h incubation (Fig. 9c, d). The present work highlights the high capacity of MOFs as an important platform in the treatment of cancer.

4. Conclusions

In this inquiry, we synthesized three MOFs with different hydrophilicity and studied the effect hydrophobicity/hydrophilicity of MOFs on the drug delivery and sensing properties. The DLC and DLE of TMU-6(RL1), TMU-21(RL2) and TMU-59, were determined by (20%, 70%), (18%, 78%) and (3.6%, 13.6%), respectively. Also, the curcumin release reached 74%, 57% and 8% for TMU-6(RL1), TMU-21(RL2) and TMU-59 after 100 h in PBS solution with pH 7.2, respectively. Studies of in vitro anticancer revealed that the cytotoxicity of the MOFs@Curcumin against HT-29 cancer cells in MOFs is more than that of free curcumin. Also, the detection limit for curcumin measurement in water is 3.6 nM for TMU-21(RL2) indicating this method as a high ranked method for curcumin analysis. In general, the results of this study showed that the tuning of MOF walls hydrophobicity/hydrophilicity as a key parameter can change the performance of these structures in drug delivery.

Declaration of Competing Interest

The authors declare that they have no known competing financial interests or personal relationships that could have appeared to influence the work reported in this paper.

Acknowledgment

This work was supported by the Natural Science Foundation of Guangxi (2018GXNSFDA281011 and 2019GXNSFDA185003), the Middle-aged and Young Teachers' Basic Ability Promotion Project of Guangxi (2021KY0702) and Tarbiat Modares University.

Appendix A. Supplementary material

Supplementary data to this article can be found online at https://doi.org/10.1016/j.arabjc.2023.104887.

References

Abedi, S., Azhdari Tehrani, A., Ghasempour, H., et al, 2016. Interplay between hydrophobicity and basicity toward the catalytic activity of isoreticular MOF organocatalysts. New J. Chem. 40, 6970–6976.
Aguado, S., Canivet, J., Schuurman, Y., et al, 2011. Tuning the activity by controlling the wettability of MOF eggshell catalysts: A quantitative structure–activity study. J. Catal. 284, 207–214.
Arora, S., Kumar, V., Kapil, L., et al, 2023. Piperine loaded metal organic frameworks reverse doxorubicin induced chemobrain in adult zebrafish. J. Control. Release S0168–3659 (0123), 00086.
Awual, M.R., 2015. A novel facial composite adsorbent for enhanced copper(II) detection and removal from wastewater. Chem. Eng. J. 266, 368–375.
Awual, M.R., 2017. New type mesoporous conjugate material for selective optical copper(II) ions monitoring & removal from polluted waters. Chem. Eng. J. 307, 85–94.
Awual, M.R., 2019a. An efficient composite material for selective lead (II) monitoring and removal from wastewater. J. Environ. Chem. Eng. 7, 103087.
Awual, M.R., 2019b. Innovative composite material for efficient and highly selective Pb(II) ion capturing from wastewater. J. Mol. Liq. 284, 502–510.
Awual, M.R., 2019c. Mesoporous composite material for efficient lead (II) detection and removal from aqueous media. J. Environ. Chem. Eng. 7, 103124.
Awual, M.R., 2019d. Novel conjugated hybrid material for efficient lead(II) capturing from contaminated wastewater. Mater. Sci. Eng. C 101, 686–695.
Awual, M.R., Hasan, M.M., Shahat, A., et al, 2015. Investigation of ligand immobilized nano-composite adsorbent for efficient cerium (III) detection and recovery. Chem. Eng. J. 265, 210–218.
Awual, M.R., Yaita, T., 2013. Rapid sensing and recovery of palladium(II) using N, N-bis(salicylidene)1,2-bis(2-aminophenylthio)ethane modified sensor ensemble adsorbent. Sens. Actuators B 183, 332–341.
Cai, M., Chen, G., Qin, L., et al, 2020. Metal organic frameworks as drug targeting delivery vehicles in the treatment of cancer. Pharmaceutics. 12, 232.
Chan, W.-H., Wu, H.-Y., Chang, W.H., 2006. Dosage effects of curcumin on cell death types in a human osteoblast cell line. Food Chem. Toxicol. 44, 1362–1371.
DeSantis, C.E., Miller, K.D., Goding Sauer, A., et al, 2019. Cancer statistics for african Americans, 2019. CA: Cancer J. Clinicians. 69, 211–233.
Fernández-Bravo, A., Figueras, M.J., 2020. An update on the genus Aeromonas: taxonomy, epidemiology, and pathogenicity. Microorganisms. 8, 129.
Gao, L.-X., Wu, D.-Z., Bigdeli, F., et al, 2020. Synthesis of a new binuclear silver (I) complex with the ability to interact with DNA molecule. Mater. Lett. 262, 127199.
Ghorbanloo, M., Tarasi, S., 2017. Vitamin B12 Controlled Release with Crosslinked Poly (Acrylic Acid) and Poly (Methacrylic Acid) Based on Chitosan and Starch as pH Sensitive Hydrogels. Lett. Drug Des. Discovery 14, 605–612.
Hasan, M., Kubra, K., Hasan, M., et al, 2023. Sustainable ligand-modified based composite material for the selective and effective cadmium(II) capturing from wastewater. J. Mol. Liq. 371, 121125.
Hasan, M.M., Shenashen, M.A., Hasan, M.N., et al, 2021. Natural biodegradable polymeric bioadsorbents for efficient cationic dye encapsulation from wastewater. J. Mol. Liq. 323, 114587.
Kim, Y., Huh, S., 2016. Pore engineering of metal–organic frameworks: introduction of chemically accessible Lewis basic sites inside MOF channels. CrstEngComm 18, 3524–3550.
Kubra, K.T., Salman, M.S., Hasan, M.N., et al, 2021a. Utilizing an alternative composite material for effective copper(II) ion capturing from wastewater. J. Mol. Liq. 336, 116325.
Kubra, K.T., Salman, M.S., Hasan, M.N., et al, 2021b. Sustainable detection and capturing of cerium(III) using ligand embedded solid-state conjugate adsorbent. J. Mol. Liq. 338, 116667.
Kubra, K.T., Salman, M.S., Znad, H., et al, 2021c. Efficient encapsulation of toxic dye from wastewater using biodegradable polymeric adsorbent. J. Mol. Liq. 329, 115541.
Larsen, P.M., Vetner, M., Hansen, K., et al, 1988. Future trends in cervical cancer. Cancer Lett. 41, 123–137.
Liu, H., Zhao, Y., Zhang, Z., et al, 2011. The effect of methyl functionalization on microporous metal-organic frameworks' capacity and binding energy for carbon dioxide adsorption. Adv. Funct. Mater. 21, 4754–4762.
Mazrouaa, A.M., Mansour, N.A., Abed, M.Y., et al, 2019. Nanocomposite multi-wall carbon nanotubes using poly(p-phenylene

terephthalamide) for enhanced electric conductivity. J. Environ. Chem. Eng. 7, 103002.
Rodríguez-Hermida, S., Tsang, M.Y., Vignatti, C., et al, 2016. Switchable surface hydrophobicity–hydrophilicity of a metal–organic framework. Angew. Chem. Int. Ed. 55, 16049–16053.
Rojas, S., Colinet, I., Cunha, D., et al, 2018. Toward understanding drug incorporation and delivery from biocompatible metal–organic frameworks in view of cutaneous administration. ACS Omega 3, 2994–3003.
Roy, S., Suresh, V.M., Maji, T.K., 2016. Self-cleaning MOF: realization of extreme water repellence in coordination driven self-assembled nanostructures. Chem. Sci. 7, 2251–2256.
Salman, M.S., Hasan, M.N., Kubra, K.T., et al, 2021. Optical detection and recovery of Yb(III) from waste sample using novel sensor ensemble nanomaterials. Microchem. J. 162, 105868.
Siegel, R.L., Miller, K.D., Fedewa, S.A., et al, 2017. Colorectal cancer statistics. CA: Cancer J. Clini. 67, 177–193.
Tarasi, S., Azhdari Tehrani, A., Morsali, A., et al, 2018a. Fabrication of amine and imine-functionalized isoreticular pillared-layer metal–organic frameworks for the highly selective detection of nitro-aromatics. New J. Chem. 42, 14772–14778.
Tarasi, S., Morsali, A., 2021. Fabrication of transparent ultraviolet blocking films using nanocomposites derived from metal-organic frameworks. J. Alloy. Compd. 868, 158996.
Tarasi, S., Tehrani, A.A., Morsali, A., et al, 2018b. Fabrication of amine and imine-functionalized isoreticular pillared-layer metal–organic frameworks for the highly selective detection of nitro-aromatics. New J. Chem. 42, 14772–14778.
Tarasi, S., Tehrani, A.A., Morsali, A., 2020. The effect of methyl group functionality on the host-guest interaction and sensor behavior in metal-organic frameworks. Sens. Actuators B 305, 127341.
Tarasi, S., Ramazani, A., Morsali, A., et al, 2021. Highly Sensitive Colorimetric Naked-Eye Detection of HgII Using a Sacrificial Metal-Organic Framework. Inorg. Chem. 60, 13588–13595.
Tarasi, S., Ramazani, A., Morsali, A., et al, 2022. Drug delivery using hydrophilic metal-organic frameworks (MOFs): effect of structure properties of MOFs on biological behavior of carriers. Inorg. Chem. 61, 13125–13132.
Xu, Z., Wu, Z., Huang, S., et al, 2023. A metal-organic framework-based immunomodulatory nanoplatform for anti-atherosclerosis treatment. J. Control. Release 354, 615–625.
Xue, J.-J., Bigdeli, F., Liu, J.-P., et al, 2018. Ultrasonic-assisted synthesis and DNA interaction studies of two new Ru complexes; RuO2 nanoparticles preparation. Nanomedicine 13, 2691–2708.
Xue, Z., Zhu, M., Dong, Y., et al, 2019. An integrated targeting drug delivery system based on the hybridization of graphdiyne and MOFs for visualized cancer therapy. Nanoscale 11, 11709–11718.
Yaghi, O.M., O'Keeffe, M., Ockwig, N.W., et al, 2003. Reticular synthesis and the design of new materials. Nature 423, 705–714.
Zheng, M., Liu, S., Guan, X., et al, 2015. One-step synthesis of nanoscale zeolitic imidazolate frameworks with high curcumin loading for treatment of cervical cancer. ACS Appl. Mater. Interfaces 7, 22181–22187.
Zhou, H., Beevers, C.S., Huang, S., 2011. The targets of curcumin. Curr. Drug Targets 12, 332–347.
Ziyatdinova, G., Nizamova, A., Budnikov, H., 2012. Voltammetric determination of curcumin in spices. J. Anal. Chem. 67, 591–594.